

Preliminary results of the High Energetic Particle Package on-board the China Seismo-Electromagnetic Satellite

Wei Chu^{1*}, JianPing Huang¹, XuHui Shen¹, Ping Wang², XinQiao Li², ZhengHua An², YanBing Xu², and XiaoHua Liang²

¹Institute of Crustal Dynamics, China Earthquake Administration, Beijing 100085, China;

²Institute of High Energy Physics, Chinese Academy of Sciences, Beijing 100049, China

Abstract: The high energetic particle package (HEPP) on-board the China Seismo-Electromagnetic Satellite (CSES) was launched on February 2, 2018. This package includes three independent detectors: HEPP-H, HEPP-L, and HEPP-X. HEPP-H and HEPP-L can detect energetic electrons from 100 keV to approximately 50 MeV and protons from 2 MeV to approximately 200 MeV. HEPP-X can measure solar X-rays in the energy range from 1 keV to approximately 20 keV. The objective of the HEPP payload was to provide a survey of energetic particles with high energy, pitch angle, and time resolutions in order to gain new insight into the space radiation environments of the near-Earth system. Particularly, the HEPP can provide new measurements of the magnetic storm related precipitation of electrons in the slot region, and the dynamics of radiation belts. In this paper, the HEPP scientific data sets are described and initial results are provided. The scientific data can show variations in the flux of energetic particles during magnetic storms.

Keywords: CSES; energetic particles; HEPP; data sets; data quality; preliminary results

Citation: Chu, W., Huang, J. P., Shen, X. H., Wang, P., Li, X. Q., An, Z. H., Xu, Y. B., and Liang, X. H. (2018). Preliminary results of the High Energetic Particle Package on-board the China Seismo-Electromagnetic Satellite. *Earth Planet. Phys.*, 2(6), 489–498. <http://doi.org/10.26464/epp2018047>

1. Introduction

To date, some electromagnetic seismic anomalies such as the disturbance of low-frequency waves, and anomalous behavior of the background plasma in the ionosphere, have been found (Parrot et al., 1985; Larkina et al., 1989; Pulinets and Boyarchuk, 2004; Pulinets, 2004; Ouzounov et al., 2018). It has also been reported that there are cases of energetic charged particles increasing before earthquakes (Chesnokov et al., 1987; Aleksandrin et al., 2003). To study the electromagnetic anomalies from space before earthquakes, electromagnetic satellites have emerged. The detectors on these satellites can usually detect the electric field, magnetic field, plasma density, and flux or spectrum of high energetic particles.

The China Seismo-Electromagnetic Satellite (CSES) (Shen XH et al., 2011; Shen XH et al., 2018) mission was successfully launched on February 2, 2018. It is the first satellite in China to measure geophysical fields. It carries eight instruments, including a search-coil magnetometer (SCM) (Cao JB et al., 2018), electric field detector (EFD), high precision magnetometer (HPM) (Cheng BJ et al., 2018), GNSS occultation receiver (GOR), plasma analyzer package (PAP), Langmuir probe (LAP), high energetic particle package (HEPP) and detector (HEPD) (Ambrosi et al., 2018), and tri-band beacon (TBB). The satellite has a sun-synchronous orbit at an altitude of 507 km

and a descending node time of 14:00 LT. The low polar orbit of the satellite and its 5-year lifetime will allow a survey of nearly all the seismically active regions and a probe of the structure of low-altitude radiation belts (Van Allen et al., 1958) during different space weather environments, which will result in numerous application prospects in seismology, geophysics, space physics, etc.

Both theory and observations have shown the correlation between variations in high-energy charged particle fluxes in near-Earth space and seismic activity. This phenomenon was pointed out for the first time at the end of the 1980 s (Chesnokov et al., 1987). The explanation of this phenomenon is based on the local disturbance of the radiation belt particle flux caused by ultra-low frequency (ULF) or very low frequency (VLF) electromagnetic emission (EME) of seismic origin (Chmyrev et al., 1989; Larkina et al., 1989; Galper et al., 1995; Sauvaud et al., 2008). Indeed, the mechanism of wave-particle interaction during the earthquakes has not been fully understood and there are some other waves, such as electromagnetic ion cyclotron waves (EMICs) and whistler mode waves (including plasmaspheric hiss and chorus wave) (Imhof et al., 1986; Abel and Thorne, 1988a, b), which are not caused by earthquakes but can also interact with energetic particles.

To obtain as much information as possible regarding energetic particles in the near Earth space, a detector of energetic particles should detect a wide energy range and have a high pitch angle resolution. This high energetic particle package (HEPP) developed by the Institute of High Energy Physics, Chinese Academy of Sciences (IHEP, CAS) includes three independent detectors: HEPP-L, HEPP-H and HEPP-X.

Correspondence to: W. Chu, chuwei4076@126.com

Received 22 OCT 2018; Accepted 05 NOV 2018.

Accepted article online 16 NOV 2018.

©2018 by Earth and Planetary Physics.

The HEPP-L detector includes nine independent sensors pointing in nine different directions intended to measure the fluxes of energetic electrons at a different pitch angle in the energy range, 100 keV–3 MeV, and the fluxes of energetic protons in the energy range 2–20 MeV. The HEPP-H detector is intended for the measurement of energetic electron fluxes within the energy range 2–50 MeV and energetic proton fluxes in the energy range 15–200 MeV. To fulfill this requirement, the maximum geometry factor of HEPP-H was designed as large as $73 \text{ cm}^2\text{sr}^{-1}$ for electrons and $90 \text{ cm}^2\text{sr}^{-1}$ for protons. A calculation of the geometric factor of the detector was performed for the complete energy range using the GEANT-4 code from CERN and hundreds of thousands of particles. HEPP-X uses silicon drift detectors (SDDs) as the X-ray radiation detector to detect X-ray spectrometry and flux. As it has high count rates and a comparatively high energy resolution (Lechner et al., 1996; Strüder and Soltau, 1995), this detector can provide information regarding the solar X-ray in the energy range of from 1 keV to approximately 20 keV with a high energy resolution which can be used to evaluate the effects of solar activities on the Earth. The HEPP payload has a sampling frequency of every one second. The main parameters of the payload are described in Table 1.

The object of the HEPP payload is to provide the best survey of energetic particles with high energy, pitch angle, and time resolutions to obtain new insight into the seismology, geophysics, space physics, and understanding of the coupling between different layers of the Earth's system.

Figure 1 shows a schematic diagram describing how the payload was installed on the satellite platform. HEPP-L and HEPP-H were installed in the Y direction and HEPP-X was installed in the Z direction, which is the zenith direction to detect the flux of solar X-rays.

The coordinates of the satellite (the red lines in Figure 1) were defined such that the X-axis is the flight direction, the Z-axis points to the center of the earth, and the Y-axis is in a right-handed coordinate relationship with the X-axis and Z-axis.

Since the successful launch of the satellite on February 2, 2018, we have had several months for the commission test. During this period we received a large amount of raw data and after the transferring function calibration we obtained the physical quantities of the observational results.

In Section 2, we present an overview of the data analysis method and briefly describe the definition of different levels of HEPP data products available through the CSES Science Data Center and also examples of the preliminary scientific results. In Section 3, comparisons are presented between HEPP detection results and res-

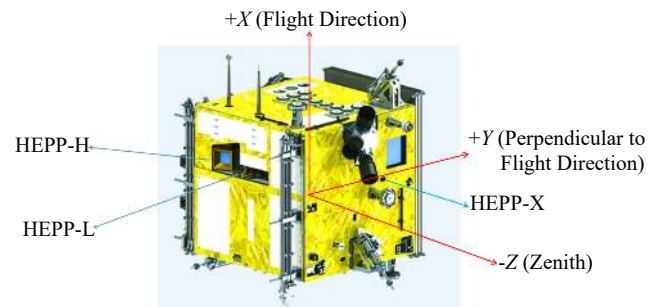


Figure 1. Schematic diagram of the HEPP installed on the satellite platform of the CSES. HEPP-L and HEPP-H were installed in the Y direction and HEPP-X in the direction which is the Zenith direction. The coordinates of the satellite (the red lines in this figure) were defined such that the X-axis is the flight direction, the Z-axis points to the center of the earth, and the Y-axis is in a right-handed coordinate relationship with the X-axis and Z-axis.

ults from observations from the Polar Operational Environmental Satellites (POES) of the National Oceanic and Atmospheric Administration (NOAA). Concluding remarks are provided in the last section.

2. HEPP Data Set Description

Generally, the scientific data of the HEPP include four different levels, from Level-1 to Level-4, that are suitable for different users. Level-1 data are for payload developers and corresponding cooperation partners, Level-2 data are for the public and the common user, while Level-3 and 4 data are suitable for researchers in the China Earthquake Administration (CEA) and other similar agencies according to the data policy of the CSES. We present here only a brief description of the four different data levels of the HEPP. The detailed format of the scientific data for all payloads on-board CSES will be described in a document that will be released during the next few months. Level-2 data will be available to guest investigators through the CSES Science Data Center operated by the Institute of Crustal Dynamics, China Earthquake Administration (ICD, CEA).

Figure 2 shows the data processing flow chart of the HEPP from the raw data to the Level 1–4 data products with all the output scientific data in the HDF5 format.

2.1 Level-0 Data

The Level-0 data are defined as the scientific data and engineering parameters of each payload from the CSES down-linked after

Table 1. Main parameters of HEPP payload

Detector	HEPP-H	HEPP-L	HEPP-X
Detection Method	Silicon detector + CsI calorimeter	Silicon semiconductor telescope array	Silicon drift chamber detector
Energy Range	e: 2–50 MeV p: 15–200 MeV	e: 0.1–3 MeV p: 2–20 MeV	X ray: 1–20 keV
Energy Resolution	10%	10%	300 eV@5.9 keV
Pitch Angle Resolution	5°	5°	-
Particle Identification	>90%	>90%	-

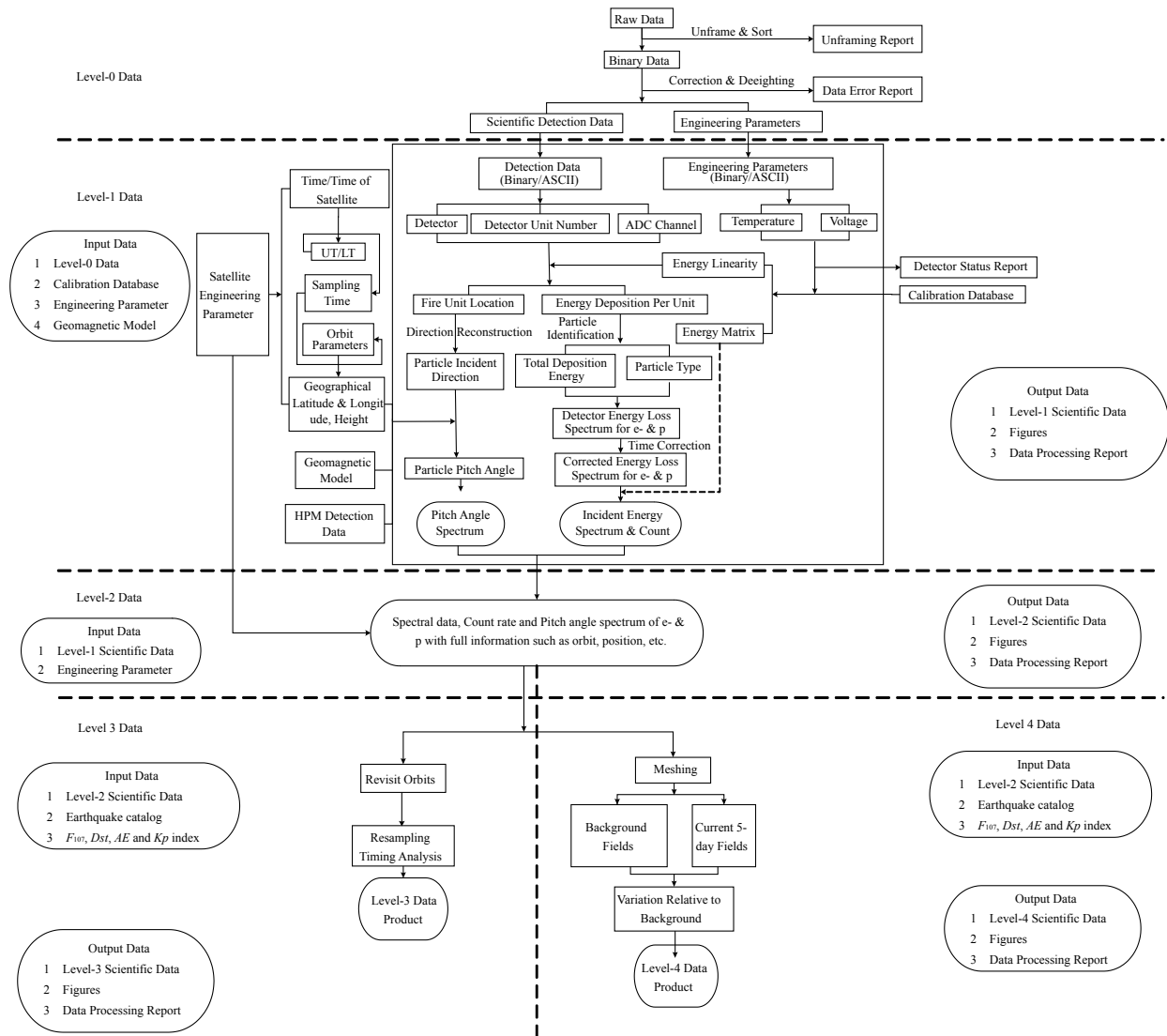


Figure 2. Data processing flow chart of the HEPP-H and HEPP-L.

descrambling, error correction, frame synchronization, and duplicate removal.

The contents of the Level-0 binary data include the operational status of the HEPP, such as temperature and voltage of the detector, and the broadcast information of the satellite, such as the GPS information, Attitude and Orbit Control System (AOCS) information, and so on. Using Level-0 data, we can monitor the health status of the detector and also obtain partial information of the satellite.

2.2 Level-1 Data

Level-1 data are defined as the physical quantities calibrated after binary-to-decimal conversion and transferring function calibration of Level-0 data.

The Level-1 data files of the HEPP include physical quantity data products, electron and proton flux, particle energy, and pitch angle, and also include case-by-case examples.

The Level-1 products of the HEPP contain time-series of quality-screened, calibrated, and corrected measurements provided in

physical SI units in geographic coordinate reference frames. Level-1 products are individually provided for each of the three detectors on a single orbit basis, i.e. each product contains all available data of that orbit range from approximately -65° to 65° latitude.

2.3 Level-2 Data

Level-2 data are defined as the physical quantities transformed from the sensor coordination system of Level-1 data into the geographic coordination system labeled with geomagnetic coordination system and satellite altitude information.

Level-2 data probably are the most important data product for the public, because Level-2 data include all the information of Level-1 data plus other information, such as the geomagnetic and geographic coordination information, which is very useful to researchers.

Simple examples illustrating pictures of HEPP-L Level-2 data of 3106 descent are shown in Figure 3. The first panel is the energy-time spectrum of the energetic electrons and the second the energy-time spectrum of protons including the X-axis labeled with

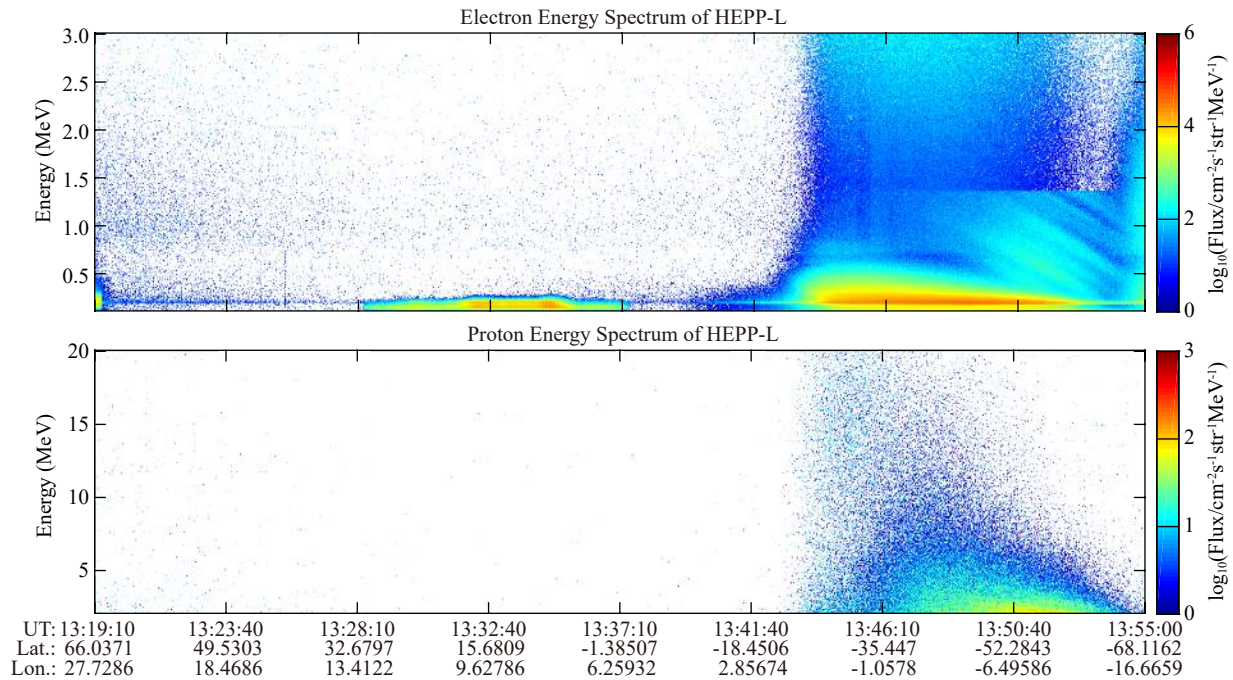


Figure 3. Simple examples illustrating pictures of HEPP-L of 3106 descent orbit. The first panel is the energy-time spectrum of the energetic electrons and the second the energy-time spectrum of protons including the X-axis labeled with the observational time and other necessary information.

the observational time and other necessary information.

2.4 Level-3 Data

Level-3 data are defined as the time series data of the half-orbit generated after resampling from Level-2 data.

In the Level-3 data, the time series data, including the particle spectrum in all directions and the flux of the particles with the selected energy, we believe have a relationship with the earthquake precursor. For the Level-3 data, the latest orbit and the statistical quantities of its revisit orbits are included in the HDF file. The statistical quantities include the median, quantiles, mean, and standard deviation of the revisit orbit data.

2.5 Level-4 Data

Level-4 data are defined as the global or regional space data retrieved from Level-2, in terms of the variation between the revisited orbits and disturbance observed according to the background field.

The spatial data of Level-4 include global and regional energetic particles spectrum data resampled from the latest full revisited period of 5 days. The background of the latest single revisit period is from the data across a time interval of more than 30 days. The statistical quantities of the background are also included in the Level-4 HDF files.

In the Level-4 PNG figure product, the global or regional map of the latest 5 days, background, and residuals of both are illustrated. Earthquakes of a magnitude greater than M 6.0 during the latest 5 days are plotted in the residuals map. The spatial intervals for resampling, flags beyond the threshold base of the statistical quantities, and other processing information are recorded in the Level-4

processing report file.

A simple example illustrating a Level-4 picture of HEPP-L is shown in Figure 4.

3. Preliminary Results of the HEPP

From the very beginning of the launch of the CSES, data from the HEPP have been sufficient to allow us to evaluate in detail the behavior of this payload.

3.1 Global Distribution of Energetic Particles

It is a reasonable to evaluate the behavior of the payload by displaying the global distribution of energetic particles, as we already have a good understanding of it. Here, we used the data during a complete revisited period from August 5 to 9, 2018, to complete this task.

During this period the space weather indexes such as the Dst index and the AE index showed that there was no geomagnetic storms or substorms that could have impacted the evaluation of the detection results. As the orbits of the satellite were designed as strictly revisited, we used interpolation for global distribution mapping of the energetic particles.

Figure 5 shows the global distribution of the energetic electrons (left) and protons (right) detected by HEPP-L during a whole revisited period from August 5 to 9, 2018. Figure 6 shows the global distribution of the energetic electrons (left) and protons (right) detected by HEPP-H using the data for the same time period. From these two figures we can see that the result is reasonable and consistent with our understanding regarding the high energy particle distribution law, both for electrons and protons in the magnetosphere.

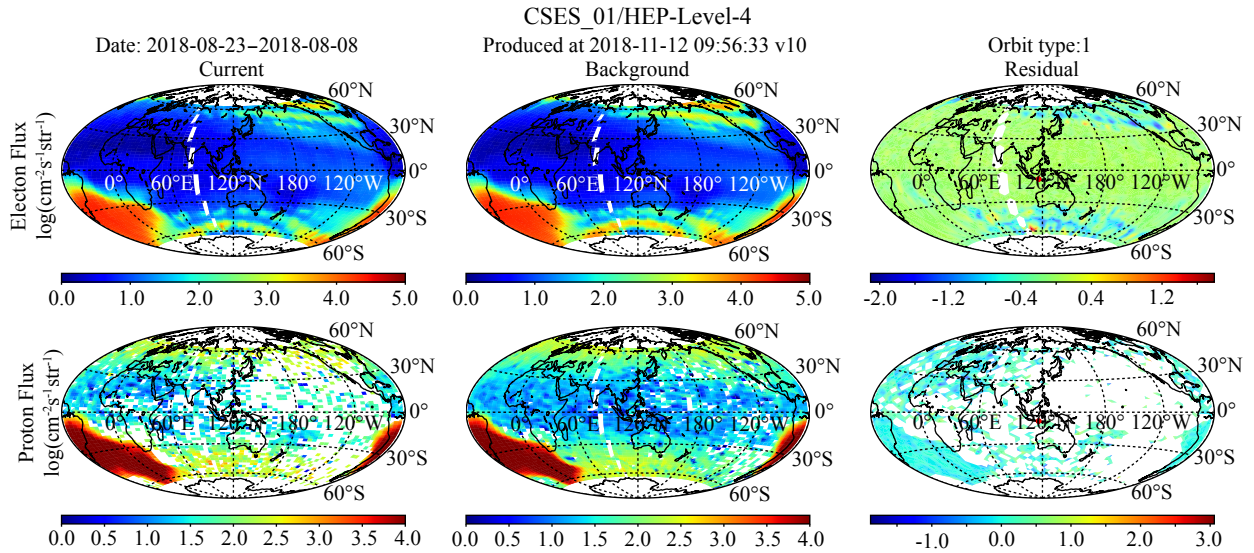


Figure 4. A simple example showing a Level-4 picture of HEPP-L. The first panel shows the current, background and the residual of the global distribution of energetic electrons. The second panel is the same as the first except that it presents the variation in protons. The white color squares indicate missing data.

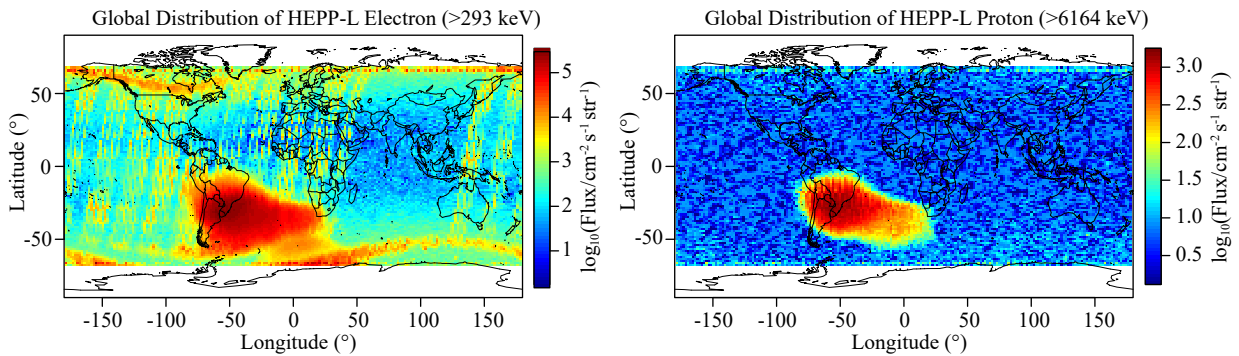


Figure 5. Global distribution of the energetic electrons (left) and protons (right) detected by HEPP-L during a whole revisited period from August 5 to August 9, 2018.

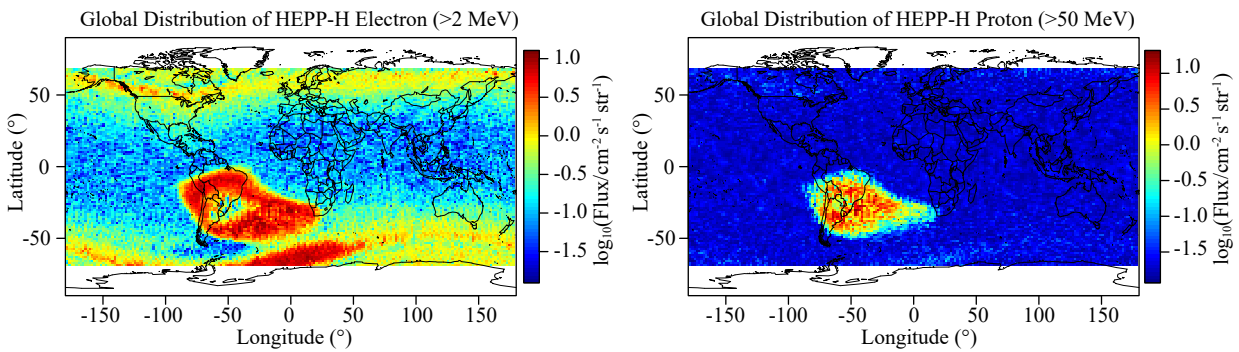


Figure 6. Global distribution of the energetic electrons (left) and protons (right) detected by HEPP-H using the data for the same time period as that of Figure 5.

HEPP-X used the silicon drift chamber method to detect X-rays. Its detection result is also a reflection of the low energetic electrons such that Figure 7 is also reasonable because the global distribution pattern is consistent with the known distribution of energetic electrons. Thus, we believe the detector is working well.

3.2 Comparison of HEPP-H and HEPP-L and the NOAA POES Satellite

To comprehensively evaluate the performance of the payload, another two comparison methods were used for further analysis. First, joint analysis between the detection results of HEPP-H and

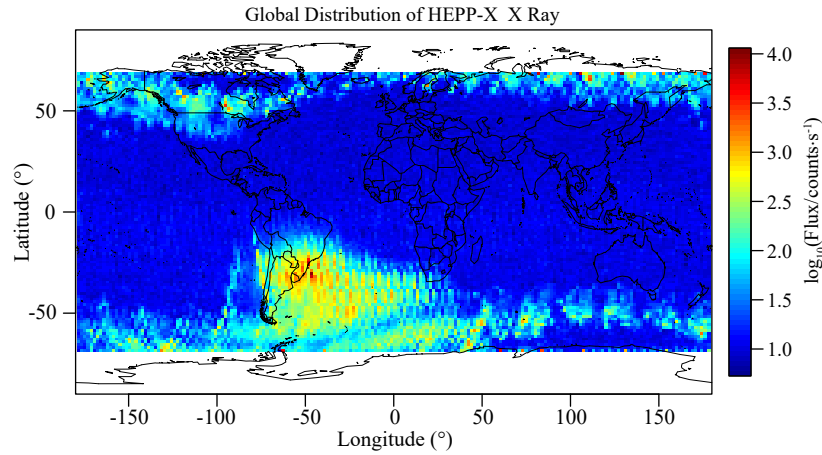


Figure 7. Detection results of HEPP-X.

HEPP-L was conducted. Then, we used the NOAA POES satellite observational data to provide a preliminary comparison.

3.2.1 Comparison to HEPP-H and HEPP-L

Both theoretical and detection results (Vasyliunas, 1961; Gosling et al., 1981; Armstrong et al., 1983; Christon et al., 1988; Divine and Garrett, 1983; Collier, 1993; Ma CY and Summers, 1998; Oka et al., 2018) show the power-law energy spectrum of the energetic particles in space plasmas such as the ionosphere, magnetosphere, and interplanetary. From main parameters of the payload listed in Table 1, we found that HEPP-H and HEPP-L can detect particles in an overlapping energy measurement range both for electrons (2–3 MeV) and protons (15–20 MeV). Furthermore, HEPP-H and HEPP-L installed on the CSES ensure that there is a

certain degree of overlap in the direction of these two detectors such that the energetic particles detected by these detectors have the same pitch angle.

In general, as HEPP-H and HEPP-L have an overlapping energy range and pitch angle, cross-validation of HEPP-L Sensors 4, 5, and 6 and HEPP-H can be conducted. The South Atlantic Anomaly (SAA) is an area with a low magnetic field which leads to an increased flux of energetic particles in this region and exposes orbiting satellites to higher-than-usual levels of radiation; this area is relatively stable and can be used to complete this task.

Here, we selected the 2417 ascend orbit data for analysis; results are shown in Figures 8 and 9.

Figure 8 and Figure 9 show the energy spectrum of the energy

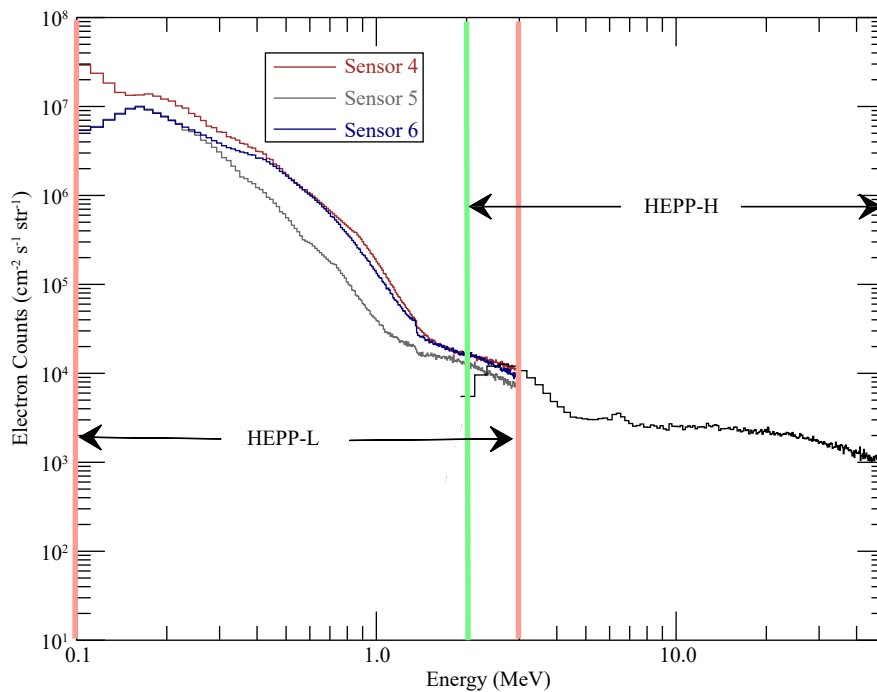


Figure 8. Energetic electron spectrum detected by HEPP-L and HEPP-H. The distribution of electrons detected by Sensors 4, 5, and 6 of HEPP-L show the power law spectrum. The results obtained by HEPP-H also show the same distribution trend.

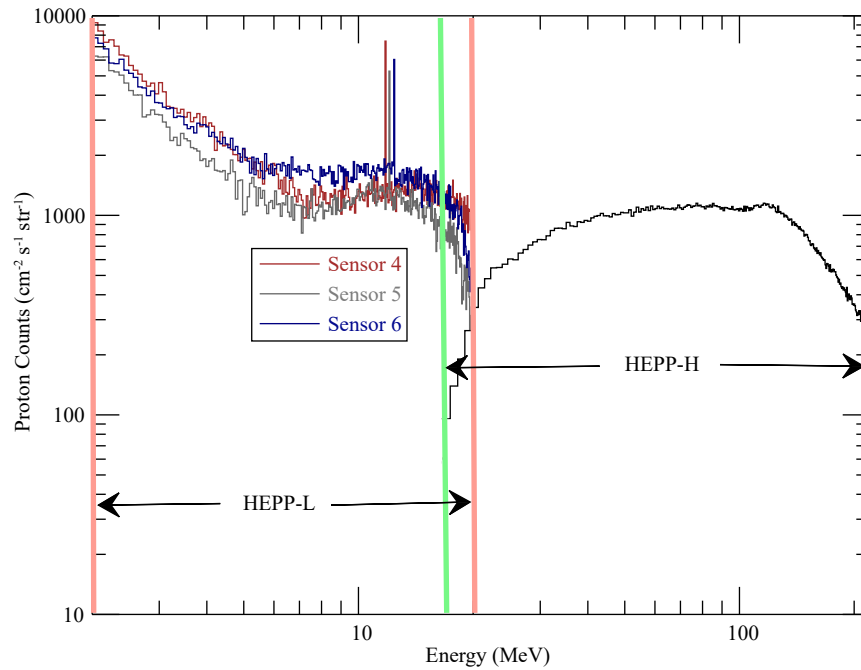


Figure 9. Energetic proton spectrum detected by HEPP-L and HEPP-H. The distribution of protons detected by Sensors 4, 5, and 6 of HEPP-L shows the power law spectrum. The results obtained by HEPP-H also show the same distribution trend.

particles obtained using the HEPP-H and HEPP-L detectors. As seen in the figures, we found that the energy spectrum is a perfect power-law spectrum, which is consistent with theoretical and previous detection results. In the overlapped energy range, the electron and proton energy spectra of these detectors are well connected and self-consistent. In the overlapping range, of low detection efficiency, the counts of the energetic particles are not exactly the same. In the future more work will be completed to solve this problem. In general, the performance of the HEPP detector is convincing.

3.2.3 Comparison to the NOAA POES Satellite

The orbits of the Polar Orbiting Environmental Satellites (POES) operated by NOAA are similar to those of the CSES while the orbital altitude is approximately 800 km and the inclination angle is 98°. All NOAA satellites (NOAA15, 18, and 19) are equipped with a suite of instruments of the Space Environment Monitor (SEM-2) (Evans and Greer, 2000) to measure the flux of energetic ions and electrons at the altitude of the satellite. The SEM2 includes two parts, which are the Total Energy Detector (TED) and Medium Energy Proton and Electron Detector (MEPED). The TED is designed to measure the energy flux carried by the auroral particles, both positively charged ions and electrons, into the polar atmosphere. The MEPED is designed to monitor the intensities of protons and electrons over a range extending from 30 keV to greater than 200 MeV with a different pitch angle according to the two detectors pointing in the 0° and 90° directions, respectively.

Here, we mainly compare and analyze the detection results of the MEPED and HEPP. As the CSES has a 5-day revisit period, complete revisit period data from August 5 to August 9, 2018, were selected for a statistical comparison analysis. Because the altitude of the CSES orbit is different from that of the POES satellite, the in-

stalled position of the HEPP probes is different from that of the MEPED, resulting in a different direction. Therefore, our comparison is limited to qualitative analysis of HEPP electrons, proton global average distribution, and MEPED observations (NOAA-15). It is impossible to have the completely same energy segment for the HEPP and MEPED. The global distribution of energetic particles of nearly the same energy range of the MEPED on-board the NOAA 15 satellite and the HEPP on-board the CSES were statistically analyzed.

For electrons, we chose the energy channel of 612 keV to compare the detection results to NOAA 15; for protons, the energy channel of 25 MeV was used to conduct comparative analysis. Figure 10 shows the global distribution of the energetic electrons detected by HEPP-L on-board the CSES (left) and the MEPED on-board NOAA 15 (right) during the same time period. In the analysis both the 0° and 90° detectors of the MEPED were used. Figure 11 shows the global distribution of the energetic protons detected by HEPP-H on-board the CSES (left) and MEPED on-board NOAA 15 (right) during the same time period.

By comparing the observations of the NOAA satellite and CSES as shown in Figure 10 and Figure 11, we found that the detection results obtained by these two payloads are consistent with each other, but there are more or less differences in the particle flux of the same energy segment. The main reasons may be that 1) the detection principle of the two is not the same, 2) the incident directions of the two detectors are different, and 3) the orbit heights of the two satellites are different. These three reasons may have caused the difference in the observational results. Considering the difference in the pitch angle and the different orbit heights, the observational results of these two detectors can be considered basically the same.

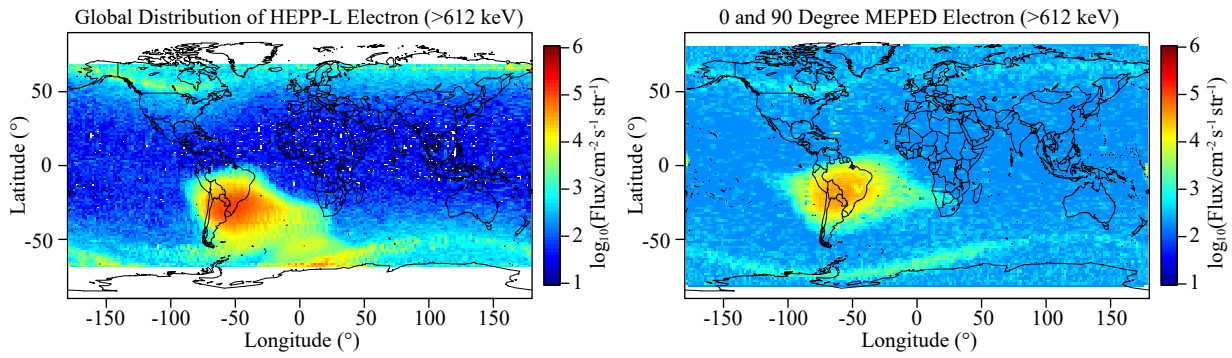


Figure 10. Global distribution of energetic electrons detected by HEPP-L on-board the CSES (left) and NOAA 15 (right) during the same time period.

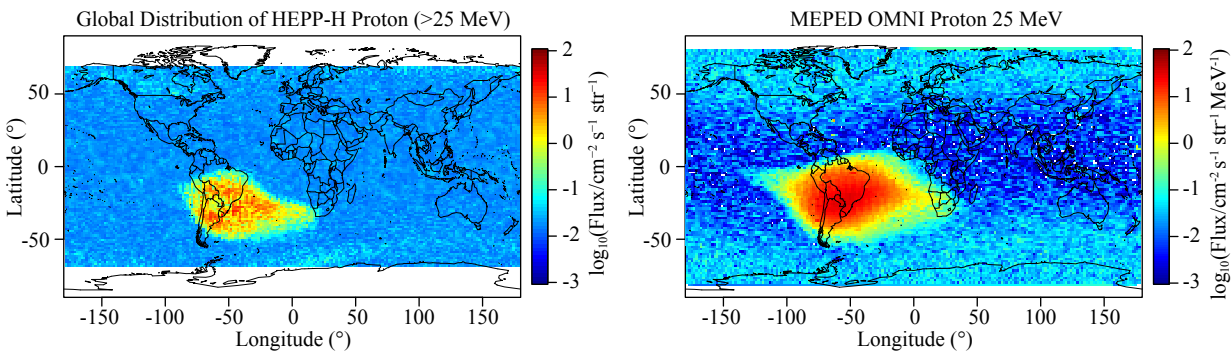


Figure 11. Global distribution of energetic protons detected by HEPP-H on-board the CSES (left) and NOAA 15 (right) during the same time period.

3.3 Geomagnetic Storm Results

On August 25, 2018, a geomagnetic storm began that lasted until August 31. From the SSC (sudden storm commencement) until the end of the recovery phase on August 31, the minimum *Dst* index during the entire process was -174 nT, which means that this storm was intense. Figure 12 shows the time variation in the *Dst* index during the storm.

By analyzing the downlink engineering parameters of the payload such as the temperature, voltage, etc., it was proved that during the whole process of the geomagnetic storm the HEPP detector remained working well. This provided us a perfect opportunity to evaluate the performance of the detector and also a good opportunity to study the transportation mechanism of high energy particles.

Figure 13 shows the energy-time spectrogram of the electrons detected by HEPP-L during the magnetic storm on August 25, 2018, from which we can see that, during the magnetic storm, the detector could detect the flux increase in the energetic electrons. The flux of the energetic electrons detected by HEPP-L rapidly varied and all electrons with a different energy increased, which means that the electrons were accelerating. In addition, many electrons were continuously injected from the magnetic tail to the orbit of the satellite.

During the initial phase, the flux of the electrons rapidly increased and during the main phase the flux of the energetic electrons remained at a high level for a period. Then, during the recovery phase, the flux of the energetic electrons maintained a high flux level consistent with theoretical and previous detection results.

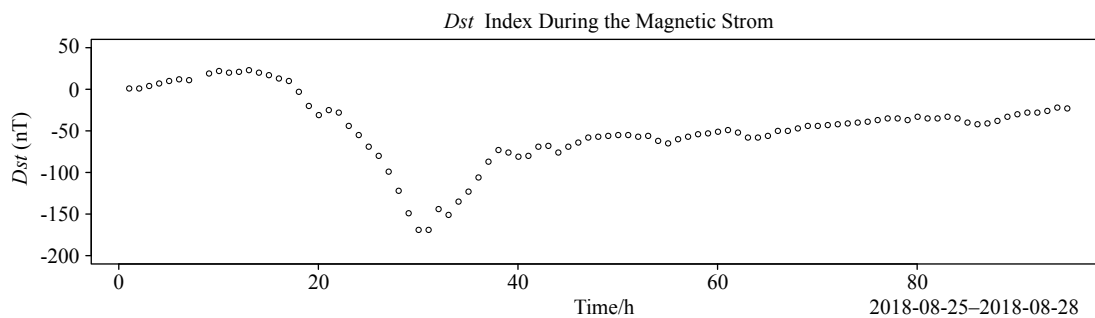


Figure 12. Time variation in the *Dst* index during the magnetic storm from August 25 to 28, 2018.

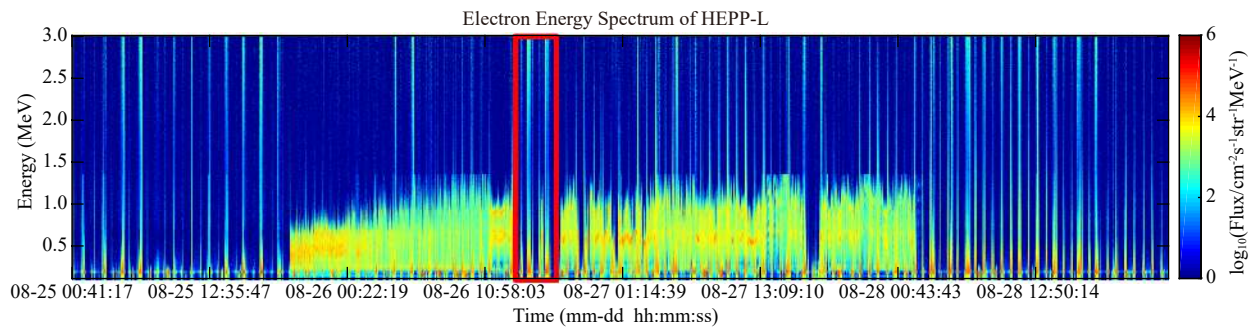


Figure 13. Energy-time spectrogram electrons detected by HEPP-L during the magnetic storm on August 25, 2018.

During the magnetic storm, there were some times when the flux of energetic particles did not maintain a high level, as shown in the red frame of the Figure 13. This is reasonable according to Reeves et al. (2003); it may be caused by the fine structure resulting from the magnetic storm, which will be studied in future research.

4. Summary and Conclusions

This study provides a brief description of the HEPP payload on-board the CSES and the scientific data set of the Application System as well as the initial results of the HEPP detection.

The HEPP payload on-board the CSES routinely provides data on the Earth's radiation belts at a low altitude within an energy range from approximately 100 keV to 50 MeV for electrons and 2 to 200 MeV for protons. The large geometrical factor and high energy and high pitch angle resolution of the HEPP allowed us to obtain new results regarding the structure of the inner radiation belt.

The scientific data of the payload, including Level-0, Level-1, Level-2, Level-3, and Level-4 data, are all described and simple example of the quick look pictures are shown.

A preliminary comparison between the HEPP detection results and those from the NOAA POES satellite SCM-2 platform was completed, from which we found that the HEPP detection results are consistent with the NOAA satellite observational results. The initial results of the magnetic storm observed are also provided, from which we found that the detector can capture the influence of the magnetic storm. This topic will be discussed in detail in future research. All results show that the HEPP payload is now working well, and the scientific data from the payload are convincing. The observed distribution of energetic particles is consistent with our understanding of space plasmas.

In the future, we will conduct joint analysis and research on the combined results of other payloads such as EFD, SCM, LAP, and PAP on-board the CSES, and also other satellites such as GOES, WIND, ACE, etc. We believe that this will be beneficial in solving the mystery of the transportation, acceleration, and loss of energetic particles in the near-ground space. These scientific data can also be used to better understand the coupling between the different layers of the Earth's system. It will also be possible to identify and detect energetic particle fluxes that are earthquake precursors, which will be very interesting and exciting.

Acknowledgment

Our work is partly supported by a research grant from the Institute of Crustal Dynamics, China Earthquake Administration (No. ZDJ2017-20). We thank Dr. Yang Wang from the School of Science, Harbin Institute of Technology, Shenzhen, for his useful discussion. Furthermore, we would like to thank our colleagues at the Institute of Crustal Dynamics, China Earthquake Administration, and also the National Space Science Data Center for providing of NOAA POES satellites Level-2 Data. Additionally, the authors also wish to thank the anonymous reviewers for their constructive comments in evaluating this paper.

References

- Abel, B., and Thorne, R. M. (1988a). Electron scattering and loss in Earth's inner magnetosphere, 1: dominant physical processes. *J. Geophys. Res.*, *103*, 2385. <https://doi.org/10.1029/97JA02919>
- Abel, B., and Thorne, R. M. (1988b). Electron scattering and loss in Earth's inner magnetosphere, 2: sensitivity to model parameters. *J. Geophys. Res.*, *103*, 2397. <https://doi.org/10.1029/97JA02920>
- Aleksandrin, S. Y., Galper, A. M., Grishantzeva, L. A., Koldashov, S. V., Maslennikov, L. V., Murashov, A. M., Picozza, P., Sgrigna, V., and Voronov, S. A. (2003). High-energy charged particle bursts in the near-Earth space as earthquake precursors. *Ann. Geophys.*, *21*(2), 597–602. <https://doi.org/10.5194/angeo-21-597-2003>
- Ambrosi, G., Bartocci, S., Basara, L., Battiston, R., Burger, W. J., Carfora, L., Castellini, G., Cipollone, P., Conti, L., ... Vitale, V. (2018). The HEPP particle detector of the CSES satellite mission for investigating seismo-associated perturbations of the Van Allen belts. *Sci. China Technol. Sci.*, *61*(5), 643–652. <https://doi.org/10.1007/s11431-018-9234-9>
- Armstrong, T. P., Paonessa, M. T., Bell II, E. V., and Krimigis, S. M. (1983). Voyager observations of Saturnian ion and electron phase space densities. *J. Geophys. Res.*, *88*(A11), 8893–8904. <https://doi.org/10.1029/JA088iA11p08893>
- Cao, J. B., Zeng, L., Zhan, F., Wang, Z. G., Wang, Y., Chen, Y., Meng, Q. C., Ji, Z. Q., Wang, P. F., ... Ma, L. Y. (2018). The electromagnetic wave experiment for CSES mission: Search coil magnetometer. *Sci. China Technol. Sci.*, *61*(5), 653–658. <https://doi.org/10.1007/s11431-018-9241-7>
- Cheng, B. J., Zhou, B., Magnes, W., Lammegger, R., and Pollinger, A. (2018). High precision magnetometer for geomagnetic exploration onboard of the China Seismo-Electromagnetic Satellite. *Sci. China Technol. Sci.*, *61*(5), 659–668. <https://doi.org/10.1007/s11431-018-9247-6>
- Chesnokov, V. Y., Galper, A. M., Kirillov-Ugryumov, V. G., Koldashov, S. V., Mikhailov, V. V., Popov, A. V., and Voronov, S. A. (1987). Registration of sporadic increase of high energy particle flux near the Brazilian anomaly region. In *Proceedings of the 20th International Cosmic Ray Conference* (pp. 451–452). Moscow: ICRC.
- Chmyrev, V. M., Isaev, N. V., Bilichenko, S. V., and Stanev, G. (1989). Observation by space-borne detectors of electric fields and hydromagnetic waves in the

- ionosphere over an earthquake centre. *Phys. Earth Planet. Inter.*, 57(1-2), 110–114. [https://doi.org/10.1016/0031-9201\(89\)90220-3](https://doi.org/10.1016/0031-9201(89)90220-3)
- Christon, S. P., Mitchell, D. G., Williams, D. J., Frank, L. A., Huang, C. Y., and Eastman, T. E. (1988). Energy spectra of plasma sheet ions and electrons from ~50 eV/e to ~1 MeV during plasma temperature transitions. *J. Geophys. Res.*, 93(A4), 2562–2572. <https://doi.org/10.1029/JA093iA04p02562>
- Collier, M. R. (1993). On generating kappa-like distribution functions using velocity space Lévy flights. *Geophys. Res. Lett.*, 20(15), 1531–1534. <https://doi.org/10.1029/93GL01702>
- Divine, N., and Garrett, H. B. (1983). Charged particle distributions in Jupiter's magnetosphere. *J. Geophys. Res.*, 88(A9), 6889–6903. <https://doi.org/10.1029/JA088iA09p06889>
- Evans, D. S., Greer, M. S. (2000). Polar orbiting environmental satellite space environment monitor-2: instrument descriptions and archive data documentation. NOAA Tech. Mem. 93, version 1.4, Boulder, CO: US Department of Commerce, National Oceanic and Atmospheric Administration, Oceanic and Atmospheric Research Laboratories, Space Environment Center.
- Galper, A. M., Koldashov, S. V., and Voronov, S. A. (1995). High energy particle flux variations as earthquake predictors. *Advances in Space Research*, 15(11), 131–134. [https://doi.org/10.1016/0273-1177\(95\)00085-5](https://doi.org/10.1016/0273-1177(95)00085-5)
- Gosling, J. T., Asbridge, J. R., Bame, S. J., Feldman, W. C., Zwickl, R. D., Paschmann, G., Scokopke, N., and Hynds, R. J. (1981). Interplanetary ions during an energetic storm particle event: The distribution function from solar wind thermal energies to 1.6 MeV. *J. Geophys. Res.*, 86(A2), 547–554. <https://doi.org/10.1029/JA086iA02p00547>
- Imhof, W. L., Voss, H. D., Walt, M., Gaines, E. E., Mabilia, J., Datlowe, D. W., Reagan, J. B. (1986). Slot region electron precipitation by lightning, VLF chorus, and plasmaspheric hiss. *J. Geophys. Res.*, 91, 8883. <https://doi.org/10.1029/JA091iA08p08883>
- Larkina, V. I., Migulin, W., Molchanov, O. A., Kharkov, I. P., Inchin, A. S., and Schvetcova, V. B. (1989). Some statistical results on very low frequency radiowave emissions in the upper ionosphere over earthquake zones. *Phys. Earth Planet. Inter.*, 57(1-2), 100–109. [https://doi.org/10.1016/0031-9201\(89\)90219-7](https://doi.org/10.1016/0031-9201(89)90219-7)
- Lechner, P., Eckbauer, S., Hartmann, R., Krisch, S., Hauff, D., Richter, R., Soltau, H., Strüder, L., Fiorini, C., ... Sampietro, M. (1996). Silicon drift detectors for high resolution room temperature X-ray spectroscopy. *Nucl. Instrum. Methods Phys. Res. A*, 377(2-3), 346–351. [https://doi.org/10.1016/0168-9002\(96\)00210-0](https://doi.org/10.1016/0168-9002(96)00210-0)
- Ma, C. Y., and Summers, D. (1998). Formation of power-law energy spectra in space plasmas by stochastic acceleration due to whistler-mode waves. *Geophys. Res. Lett.*, 25(21), 4099–4102. <https://doi.org/10.1029/1998GL900108>
- Oka, M., Birn, J., Battaglia, M., Chaston, C. C., Hatch, S. M., Livadiotis, G., Imada, S., Miyoshi, Y., Kuhar, M., ... Retinò, A. (2018). Electron power-law spectra in solar and space plasmas. *Space Sci. Rev.*, 214(5), 82. <https://doi.org/10.1007/s11214-018-0515-4>
- Ouzounov, D., Pulinet, S., Hattori, K., and Taylor, P. (2018). *Pre-Earthquake Processes: A Multidisciplinary Approach to Earthquake Prediction Studies*. Washington: John Wiley & Sons.
- Parrot, M., Lefeuvre, F., Corcuff, F. Y., and Godefroy, P. (1985). Observations of emissions at the time of earthquakes in the Kerguelen 1985 Modelling the ionospheric disturbance caused by an explosion on the ground. *Ann. Geophys.*, 3, 695–704.
- Pulinets, S., and Boyarchuk, K. (2004). *Ionospheric Precursors of Earthquakes*. Berlin Heidelberg: Springer Science & Business Media.
- Pulinets, S. (2004). Ionospheric precursors of earthquakes; recent advances in theory and practical applications. *Terr. Atmos. Oceanic Sci.*, 15(3), 413–435. [https://doi.org/10.3319/TAO.2004.15.3.413\(EP\)](https://doi.org/10.3319/TAO.2004.15.3.413(EP))
- Reeves, G. D., McAdams, K. L., Friedel, R. H. W., and O'Brien, T. P. (2003). Acceleration and loss of relativistic electrons during geomagnetic storms. *Geophys. Res. Lett.*, 30(10), 1529. <https://doi.org/10.1029/2002GL016513>
- Sauvaud, J. A., Maggiolo, R., Jacquey, C., Parrot, M., Berthelier, J. J., Gamble, R. J., and Rodger, C. J. (2008). Radiation belt electron precipitation due to VLF transmitters: Satellite observations. *Geophys. Res. Lett.*, 35(9), L09101. <https://doi.org/10.1029/2008GL033194>
- Shen, X. H., Zhang, X. M., Wang, L. W., Chen, H. R., Wu, Y., Yuan, S. G., Shen, J. F., Zhao, S. F., Qian, J. D., and Ding, J. H. (2011). The earthquake-related disturbances in ionosphere and project of the first China Seismo-Electromagnetic Satellite. *Earthq. Sci.*, 24(6), 639–650. <https://doi.org/10.1007/s11589-011-0824-0>
- Shen, X. H., Zhang, X. M., Yuan, S. G., Wang, L. W., Cao, J. B., Huang, J. P., Zhu, X. H., Piergiorgio, P., and Dai, J. P. (2018). The state-of-the-art of the China Seismo-Electromagnetic Satellite mission. *Sci. China Technol. Sci.*, 61(5), 634–642. <https://doi.org/10.1007/s11431-018-9242-0>
- Strüder, L., and Soltau, H. (1995). High resolution silicon detectors for photons and particles. *Radiat. Prot. Dosim.*, 61(1-3), 39–46. <https://doi.org/10.1093/oxfordjournals.rpd.a082751>
- Van Allen, J. A., Ludwig, G. H., Ray, E. C., and McIlwain, C. E. (1958). Observation of high intensity radiation by satellites 1958 Alpha and Gamma. *J. Jet Propul.*, 28(9), 588–592. <https://doi.org/10.2514/8.7396>
- Vasyliunas, V. M. (1968). A survey of low-energy electrons in the evening sector of the magnetosphere with OGO 1 and OGO 3. *J. Geophys. Res.*, 73(9), 2839–2884. <https://doi.org/10.1029/JA073i009p02839>